AD-A067 940 JOHNS HOPKINS UNIV LAUREL MD APPLIED PHYSICS LAB F/G 3/2
NEW UNDERSTANDING OF ENERGETIC PARTICLE PROPAGATION IN THE MAGN--ETC(U)
OCT 78 E C ROELOF, R E GOLD N00024-78-C-5384
UNCLASSIFIED SCIENTIFIC-3 AFGL-TR-78-0293 NL

| OF |
AD
A067940

END
DATE
FILMED
6 -79
DDC

AFGL-TR-78-0293

LEVEL II

NEW UNDERSTANDING OF ENERGETIC PARTICLE PROPAGATION IN THE MAGNETIC FIELDS OF THE SOLAR CORONA AND INTERPLANETARY MEDIUM

E.C. Roelof
R.E. Gold

The Johns Hopkins University
Applied Physics Laboratory
Laurel, Maryland 20810

Scientific Report No. 3

October 1978

AIR FORCE GEOPHYSICS LABORATORY
AIR FORCE SYSTEMS COMMAND
UNITED STATES AIR FORCE
HANSCOM AFB, MASSACHUSETTS 01731

Unclassified

SECURITY CLASSIFICATION OF THIS PAGE (When Data Entered)

(19) REPORT DOCUMENTATION PAGE	READ INSTRUCTIONS BEFORE COMPLETING FORM
(18) 1. REPORT NUMBER: AFGL-TR-78-0293	2. GOVT ACCESSION NO.
	3. RECIPIENT'S CATALOG NUMBER (14)
(6) 4. TITLE (and Subtitle): New Understanding of Energetic Particle Propagation in the Magnetic Fields of the Solar Corona and Interplanetary Medium.	5. TYPE OF REPORT & PERIOD COVERED: Scientific [redacted]-3
	6. PERFORMING ORG. REPORT NUMBER
(10) 7. AUTHOR(s): E. C. Roelof [redacted] R. E. Gold	8. CONTRACT OR GRANT NUMBER(s): MIPR FY7121600002 (15) N00024-78-C-5384
9. PERFORMING ORGANIZATION NAME AND ADDRESS: The Johns Hopkins University, Applied Physics Laboratory, Laurel, Maryland 20810	10. PROGRAM ELEMENT, PROJECT, TASK AREA & WORK UNIT NUMBERS: 61102F (16) 2311G1AI (17) G1
11. CONTROLLING OFFICE NAME AND ADDRESS: Air Force Geophysics Laboratory, Hanscom AFB, Massachusetts 01731, Monitor/M. A. Shea/PHG	(11) 12. REPORT DATE: Oct [redacted] 78
	13. NUMBER OF PAGES: 33
14. MONITORING AGENCY NAME & ADDRESS (if different from Controlling Office) (12) 33p.	15. SECURITY CLASS. (of this report): Unclassified
	15a. DECLASSIFICATION/DOWNGRADING SCHEDULE

16. DISTRIBUTION STATEMENT (of this Report)

Approved for public release; distribution unlimited

17. DISTRIBUTION STATEMENT (of the abstract entered in Block 20, if different from Report)

18. SUPPLEMENTARY NOTES

Work performed as Task ZF10 of Contract N00024-78-C-5384 (formerly Contract N00017-72-C-4401), Department of the Navy. Continues work previously performed under MIPR No. FY71217700005 and MIPR No. FY71217600002.

19. KEY WORDS (Continue on reverse side if necessary and identify by block number)

20. ABSTRACT (Continue on reverse side if necessary and identify by block number)

Significant improvements in understanding coronal and interplanetary propagation of energetic particles are summarized, and their relationship to prediction techniques is indicated. Observational and theoretical evidence is drawn from synoptic compilations of solar activity and coronal magnetic structure as well as syntheses of plasma, field and energetic particle observations between 1 and 6 AU, utilizing both solar and Jovian particles as probes of the heliosphere.

DD FORM 1 JAN 73 1473 EDITION OF 1 NOV 65 IS OBSOLETE

Unclassified 031 650

SECURITY CLASSIFICATION OF THIS PAGE (When Data Entered)

1. INTRODUCTION

A045 021

In Scientific Report No. 2 (AFGL-TR-77-0166) we identified nine scientific subjects (closely related to prediction of solar-terrestrial disturbances) which we were pursuing at that time. That effort led to the publication of nine papers in 1976-7: three in refereed journals and six in conference proceedings.

This year, we focused on eight of those nine subjects (having completed for the present our investigations of interplanetary radio scintillations). The results have taken us another significant step closer toward reliable prediction techniques.

Coronal magnetic fields

Origin of solar wind streams

Coronal propagation of energetic particles

Sources of heavy ion enhancements in solar particle events

Synthesis of solar and interplanetary plasma, magnetic field and energetic particle observations

Interplanetary propagation and interaction of solar energetic particles with the Earth's magnetosphere

Interplanetary propagation of relativistic Jovian electrons

Energetic particle bursts in the magnetotail and upstream of the bow shock

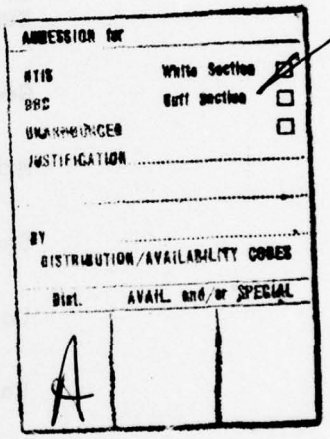

The joint efforts with our colleagues at JHU/APL and collaborating institutions resulted in the submission for publication of ten articles cited for support under this contract: five in refereed journals, three in UAG Special Reports, and two in conference proceedings. Co-authors at JHU/APL were S. M. Krimigis, D. G. Mitchell and R. D. Zwickl, while authors from other institutions were:

American Science and Engineering
J. T. Nolte, J. M. Davis

Ames Research Center/NASA
J. H. Wolfe

Loyola College (Baltimore)
J. M. Hanson (student)

Space Environment Laboratory/NOAA
P. S. McIntosh

University of Iowa
W. M. Cronyn, J. J. Rickard and S. D. Shawhan

University of Kansas
T. P. Armstrong

The scientific results of these articles are summarized in Section 2 of this report. Other collaborations undertaken this year, involved the following scientists at other institutions (most of whom were also visitors to JHU/APL):

Center for Astrophysics (Harvard)
R. H. Levine

European Space Research and Technology Centre
R. Reinhard

Georgetown University
A. Prakash

McMath-Hulbert Observatory (U of Michigan)
H. W. Dodson Prince, E. R. Hedeman, O. C. Mohler

Space Environment Laboratory/NOAA
D. J. Williams

University of California at San Diego
R. W. Fillius

University of Kiel (West Germany)
G. Green

The effort at McMath-Hulbert (described in the next section), was supported by a sub-contract, while J. M. Hanson and A. Prakash were supported at JHU/APL.

We presented eight contributed papers to the American Geophysical Union: three at the Fall National Meeting in San Francisco, December 5-9, 1977; and five at the Spring National Meeting in Miami, April 17-21, 1978. Four invited papers were presented at different meetings, all of which will appear in published form:

Roelof, E. C., The 'scatter-free' approximation for cosmic ray transport in the inner heliosphere, American Geophysical Union, Miami, April 17-21, 1978.

Roelof, E. C. and R. E. Gold, Prediction of solar energetic particle event histories and geomagnetic disturbances using real-time particle and solar wind measurements, NATO/AGARD Symposium on Operational Modeling of the Aerospace Propagation Environment; Ottawa, April 24-28, 1978.

Roelof, E. C., S. M. Krimigis and R. E. Gold, Coronal propagation and storage at energies ~ 1 MeV/nucleon, Solar Probe Science Workshop, Pasadena, May 22-23, 1978.

Roelof, E. C., Solar energetic particles: From the corona to the magnetotail, AGU Chapman Conference on 'Quantitative Modeling of Magnetospheric Processes, La Jolla, Sept. 18-22, 1978.

2. SUMMARY OF SCIENTIFIC RESULTS

We begin our summary with a graphical attempt to show why such apparently diverse subjects as those listed in the Introduction are actually all inter-related to the question of how solar plasma, magnetic field and energetic particles are transported from the sun to the Earth, and hence related to the question of solar-terrestrial disturbance prediction.

Figure 1 indicates the regime of the heliosphere analyzed in each of the ten studies we completed this year. The author lists refer to the articles described below. We present a brief summary of the most important results from each paper along with the most appropriate figure(s) from that paper.

SOLAR ACTIVITY

Particle acceleration has its origin in solar activity. *Hanson, Gold and Roelof, 1978* have compiled Solar Activity Charts for the Skylab period (Carrington Rotations 1600 - 1611) of selected indices of optical solar flares, radio bursts, soft x-rays and 2 - 5 MeV protons measured by IMP-7 and 8 in a concise graphical form. The charts were initially designed to complement studies of the coronal and interplanetary distribution of energetic solar particle populations, although their compact representation of spatial and temporal relationships has been of assistance in a wide variety of solar-terrestrial studies. The charts show the H_α importance and brightness of confirmed flares, the 1-8 Å peak x-ray flux and a spectral average of decimetric radio emissions related to the optical flares. Full disk coverage extends from April 13, 1973 through 24 February 1974.

The energetic particle fluxes are represented on the charts as a continuous swath centered on the estimated high coronal connection longitude of the large scale interplanetary field line from earth. The width of the swath is proportional to the logarithm of the $\sim$ 3 MeV proton flux measured at earth. The charts are organized in heliographic longitude versus time so it is easy to follow the development of an active region throughout its disk passage on a given solar rotation as well as its recurrences over several rotations, since all the activity from a given region falls on a straight vertical line. Conversely, all the flares and related radio and x-ray bursts on the disk at a given time are distributed along a horizontal line. The charts also indicate directly the distance between an active region and the

longitude where energetic protons (associated with activity in that region) were injected onto the interplanetary field lines leading to the earth. Figure 2 shows the Solar Activity Chart for Rotation 1604.

This representation provides an effective insight into the space/time "cut" of the sun sampled by field lines from Earth. *Dodson-Prince and Hedeman* have developed a complementary representation and an additional graphical summary of solar-terrestrial activity which was first reported in AFGL-TR-77-0222 for the year 1970. They have augmented their analysis for 1970 and are proceeding into the years 1971-2 under a subcontract to this effort.

CORONAL MAGNETIC FIELDS

Since coronal magnetic fields control the emission of solar wind as well as the transport and escape of energetic particles, "charts" of the coronal structure contain fundamental information for solar-terrestrial relationships. Consequently *P. S. McIntosh* of the Space Environment Laboratory of NOAA, working over the past seven years with personnel supported by AFGL contracts, has edited an annotated atlas of H_α Synoptic Charts *(McIntosh, 1978)* which delimit large-scale magnetic polarity regions in the low corona. The Atlas covers most of Solar Cycle 20 (Carrington Rotations 1487 - 1617). During the Skylab period, American Science and Engineering soft x-ray photographs revealed loop structures which augment the information in H_α Synoptic Charts and heliomagnetograms. *Hanson and Roelof (1978)* have compiled a comprehensive atlas of these emission structures for Carrington Rotations 1601-1610 to serve as a basis for detailed analysis of solar particle events.

Large-scale ($\sim 10^\circ$) emission features visible in soft x-ray photographs from the spectrographic telescope S-054 on Skylab have been superposed on H_α Synoptic Charts *(McIntosh, 1978)*. The charts identify loop arcades and loop complexes associated with strong magnetic fields, as well as coronal holes and areas devoid of emission loops. Although not adequate for the study of the geometry of individual features, the charts convey a global sense of coronal structure which is often difficult to obtain from individual (disc) images.

The x-ray structures read from disc photographs were located in heliographic latitude and longitude on the H_α Synoptic Charts. Figure 3a is the H_α Synoptic Chart of Carrington Rotation 1604 in July-August 1974 *(McIntosh, 1978)*. Figure 3b shows the end points of x-ray loops with dashed lines

connecting them and x-ray plages as striped regions. The areas of coronal holes from published atlases are stippled. Figure 3c shows the superposition of the x-ray loops on the H_α chart.

CORONAL PARTICLE PROPAGATION

Roelof, Krimigis and Gold (1978) have demonstrated (using solar wind mapping of interplanetary field lines), that coronal magnetic fields can produce rather well—ordered energetic particle emission profiles (e.g., over equatorial coronal holes). *Zwickl et al. (1978)* identified the eastern boundary of a solar wind stream in the vicinity of a nearby active region as a likely escape location for small solar particle events enriched in high-Z ions during the years 1972-76 at the end of Solar Cycle 20. Using Mariner 4 data from the very beginning of Solar Cycle 20, *Roelof et al. (1978)* concluded that low energy protons often escaped the corona preferentially from open magnetic structures remote ($> 60^\circ$) from the likely acceleration site, but these open structures seldom served as sources of high speed solar wind streams.

Roelof, Krimigis and Gold (1978) discussed representative energetic particle events related to quasi-stationary particle populations, solar flare events and solar composition. These events were discussed in the context of similar observations likely to be made during the proposed Solar Probe mission. Particular emphasis was given to inter-relationships with coronal magnetic structure and plasma processes. Figures 4 and 5 from *Levine and Roelof (1978)* elucidate some of these relationships. Figure 4 shows the coronal magnetic structure in the vicinity of a small equatorial coronal hole as deduced from observations by the AS&E soft x-ray telescope on Skylab and from potential field calculations based on photospheric observations. Figure 5 shows that there is a quasi-stationary depression in the low energy solar proton population on interplanetary field lines that map back to the vicinity of the coronal hole.

Zwickl et al. (1978) conducted a detailed investigation of the relationships between coronal structure and the release into interplanetary space of medium and heavy ion nuclei. A systematic analysis of the hourly

average $Z \geq 3$ rate data (September 1972-December 1976) measured with the JHU/APL IMP-7 and 8 detectors revealed 13 short-lived events that had greatly enhanced $Z \geq 3$ fluxes. In addition to confirming the results of earlier studies that all ^{3}He-rich events are Fe-rich but not vice versa, they found that these 13 enriched events had several remarkable characteristics: (1) they are generally not associated with *major* solar flares but appeared to be associated with low levels of activity (sub-flares) in western hemisphere solar active regions that are located very close to the spacecraft's high coronal interplanetary magnetic field connection longitude; (2) they had very large and prolonged outward streaming anisotropies, sometimes persisting ~ 1 day; (3) the spectral indices measured for p, α and $Z \geq 3$ particles during the times of maximum flux for the Z-rich events were identical within errors to those measured in large flare events, while small impulsive and corotating events generally showed a softer spectrum; and (4) Z-rich events appear to be associated with the low speed wind that precedes the onset of solar wind streams. Figure 6 shows a topographical map of the observed solar and interplanetary phenomena for the average Z-rich event shown as a function of radial distance and heliographic longitude. Included are the approximate locations of the solar flare active region, the coronal transition region denoted by the Alfvén critical surface, the fast and slow speed solar wind compression and rarefraction region (shaded) and the observed Z-rich event.

They concluded from this study that the same type of acceleration process that is responsible for the large proton events if responsible for the small Z-rich events, and therefore that the $Z \geq 3$ and ^{3}He enrichments are more likely due to enhanced abundances in the pre-accelerated plasma rather than to preferential enrichment during the acceleration process. This interpretation is complementary to recent findings concerning abundances and coronal emission structure of low-speed solar wind. They concluded that compositional studies of low energy solar particle events offer a good diagnostic of the flare acceleration process and possible inhomogeneities in the solar atmosphere, suggesting that solar composition maybe quite variable on a global scale.

Roelof et al. (1978) examined the influence of coronal magnetic fields on energetic particle release during solar minimum. They presented a comprehensive synthesis of interplanetary and solar data taken in conjunction

with the energetic solar proton events observed on Mariner 4 during the first eight months of 1965. They found that regions of preferential escape of energetic particles into the interplanetary medium tend to recur, even though the sites of acceleration of the particles were generally different on successive rotations. They suggested that the particles were transported in high magnetic arcades to the coronal "escape regions", and that the magnetic field line topology in these regions, although open, were fundamentally different from that of the fastest solar wind stream sources during the same period. These results are summarized in Figure 7 which depicts the temporal and spatial relationships observed during the first eight-solar rotations in 1965. The recurrent event series are labelled by a letter and occurrence number. The panels in Figure 7 show two events from each of the series. Panels consist of segments of H_α synoptic charts, with regions of well-defined negative magnetic polarity shaded. Most likely active region particle sources are marked by heavy dots. Regions of escape of energetic particles are marked by bars at the heliographic latitude of Mariner 4, with positive (vertical lines), negative (horizontal lines) or mixed (both) interplanetary polarity also indicated. The escape regions for energetic particles are shown in the panels as horizontal bars with observed boundary edges marked by vertical ends, while boundaries not observable because of temporal changes in particle intensities have pointed ends. Solar wind "dwells" (i.e., eastern boundaries of solar wind stream sources) are marked by heavy brackets (velocity > 400 km/s) or curved lines (velocity < 400 km/s) which are dashed for temporal streams. The relative stability of the energetic particle escape regions as well as their displacement from the solar wind stream sources are clearly shown in the figure.

ORIGIN AND STRUCTURE OF SOLAR WIND STREAMS

Mitchell et al. (1978) compared solar wind velocity structure mapped back to the sun from Pioneer 10 and 11 as far as ~ 5 AU with that mapped back from Earth to deduce strong latitudinal gradients. Moreover, they showed that these structures agreed with the general shape of coronal magnetic polarity regions for series of recurrent streams from Carrington Rotations 1587-1641 (March 1972 to April 1976). Spacecraft data were taken from IMP 7/8 at earth, Pioneers 6, 8 and 9 near 1 AU, and Pioneers 10 and 11 between 1.6 and 5 AU.

Using the constant radial velocity solar wind approximation to map all of the velocity data to its high coronal emission heliolongitude, they examined the velocity structure observed at different spacecraft for latitudinal dependence and compared it with coronal structure in soft x-rays and H_α absorption features. They found that the constant radial velocity approximation usually remains self-consistent in decreasing or constant velocity solar wind out to 5 AU, which enabled them to separate radial from latitudinal propagation effects. They deduced several examples of sharp non-meridional stream boundaries in interplanetary space ($\sim 5^\circ$ latitude in width), often directly associated with features in coronal x-rays and H_α. In one structure there was evidence for significant (up to 40°) non-radial flow of the plasma in the corona below the altitude of transition to super-Alfvénic flow.

Mitchell et al. (1978) also presented explanations for the diffuse boundaries that are occasionally seen at the eastern edge of solar wind streams. Their inferred velocity structure with nearly azimuthal boundaries is depicted schematically in Figure 8 along with the solar wind velocoty profiles observed at Pioneer 11 and IMP 7/8 for solar rotation 1610. The structure to the right of the coronal hole cannot be accurately deduced due to stream-stream interactions. To the left (east) the Pioneer 11 velocities drop much more quickly than the IMP 7/8 velocities. The structure sketched is consistent with the observations (including the interplanetary magnetic field polarity agreement with that in the hole), but other geometries are not excluded.

INTERPLANETARY PROPAGATION AND INTERACTION WITH THE MAGNETOSPHERE

Zwickl and Roelof (1978), using < 1 MeV proton anisotropy data from IMP-7 and 8, have demonstrated that the dominant mechanism for interplanetary transport of these particles transverse to the magnetic field is simply the $\underline{E} \times \underline{B}$ drift, i.e., the particle guiding centers stay on the "same" field line without measureable transverse scattering. In order to draw these conclusions on interplanetary propagation, they identified and quantitatively compensated for several effects due to proximity to the magnetosphere (e.g., reflection of particles and magnetospheric bursts). Their results further validate the field-line mapping technique described by *Roelof and Gold (1978)* which is central to the prediction of the history of energetic particle events.

Zwickl and Roelof (1978) examined all non-impulsive energetic particle events observed by the JHU/APL detectors on IMP-7/8 from 1972-75. After applying selection criteria to reduce magnetospheric influence to a minimum they had 1289 hourly anisotropy averages for which they also had simultaneous hourly averaged solar wind and magnetic field data.

These anisotropy vectors were resolved into components parallel and perpendicular to the measured magnetic field. The resulting anisotropy distributions led directly to the following model-independent conclusions. (1) The parallel anisotropy component averages nearly to zero, indicating virtually no net particle flow along the field line at 1 AU. (2) The average perpendicular anisotropy component is entirely accounted for in terms of the $\underline{E} \times \underline{B}$ drift, and hence transverse diffusion is negligible at these energies; application of the diffusion model to the data implies $\lambda_\perp/\lambda_\parallel \leq 0.02 \pm 0.05$ where $\lambda_\parallel$ and $\lambda_\perp$ represent the diffusion mean free path parallel and perpendicular to $\underline{B}$. (3) The net flow of particles, observed by spacecraft located at 1 AU, is outward away from the sun in a direction approximately perpendicular to the average magnetic field; if the particle populations are considered to be quasi-stationary (i.e., "corotating"), this directly implies that the effective source for these particles lies inside 1 AU.

Figure 9 shows the degree of precision that *Zwickl and Roelof (1978)* were able to achieve in their analysis. The figure shows scatter plots of the calculated $\underline{E} \times \underline{B}$ drift anisotropy $\underline{\eta}_\perp$ versus the measured anisotropy component perpendicular to the magnetic field direction $\underline{\xi}_\perp$ in geocentric solar ecliptic coordinates. The $\underline{\xi}_\perp$ and $\underline{\eta}_\perp$ data show an amazingly strong correlation which suggests that the propagation of low energy protons is well described by collimated convection.

Roelof and Gold (1978) assumed that energetic particle propagation could be described by collimated convection and examined its application to the decay of solar particle events. Once a solar particle event has begun, prediction estimates of the subsequent flux history of the maximum and decay phase of the event can be derived from real-time particle flux and solar wind velocity measurements. The solar wind velocities define the instantaneous solar longitude of the coronal foot-point of the interplanetary magnetic field

lines which the charged particles must follow to the earth. The particle event history is often dominated by changes in this coronal "connection longitude" since there are strong gradients in the coronal energetic particle populations. However, when particle fluxes are "mapped back" to their coronal connection longitude, a relatively simple coronal longitude profile and injection history is revealed. When identified in real time, these coronal signatures allow forecasts of the subsequent history of the event.

Protons $\sim$ 300 keV have proven to be sensitive indicators of coronal particle populations and interplanetary propagation conditions at higher energies as well. Hence monitoring of 300 keV protons also facilitates prediction of $\sim$ 10 MeV/nuc proton and alpha fluxes. The flux forecasts are contingent upon solar wind structure, and therefore can be up-dated continually from the real-time spacecraft solar wind data or interplanetary radio scintillation observations. They presented analyses of several solar particle events from Solar Cycle 20 and demonstrate the technique through a real-time prediction scenario for each event. Figure 10 schematically shows how a stationary energetic particle stream with a longitude profile as shown in panel a may be distorted by a solar wind stream which rises early (panel b) or late (panel c) during the event. The lower panel shows how the connection longitude of the observer changes with time for the above cases.

JOVIAN ELECTRONS

Regarding Jupiter as a source of test particles (energetic electrons) to probe the outer heliosphere, *Gold and Roelof (1978)* have presented a new model for propagation in which the solar wind stream-stream interaction regions form "diffusive walls" to "scatter-free cavities". Evidence for their model is drawn from the relationship of Jovian electrons "events" and solar wind stream structure observed between 1 and 6 AU. This Jovian electron study has led to a new propagation model that must apply to all particles in the heliosphere (Jovian, galactic, or solar), which had not been obtained from solar or galactic particle measurements alone.

This model is based on the large solar wind stream interaction regions, discovered during the Pioneer 10 and 11 missions. They continue to thicken with heliocentric distance and close off between $\sim$ 8 and 12 AU, dividing the heliosphere into cavities of relatively undisturbed plasma surrounded by more

turbulent interaction regions. It is proposed that Jovian electrons propagate nearly scatter-free within the cavities, but diffusively in the surrounding stream interaction regions which form the cavity walls. The diffusive-walled-cavity model predicts all of the observed relationships between Jovian electron events and solar wind stream structure identified at 1 AU during 1966-1976 as well as those observed by Pioneers 10 and 11 out to > 10 AU. The model also predicts a radial gradient in the intensity of electron events beyond 5 AU that falls off with distance R from the planet significantly slower than R^{-1}, as observed. The abrupt decrease in electron flux observed by Pioneer 10 at ~ 5.7 AU suggests that the effective electron emission region in the Jovian magnetotail is ≤ 1 AU in length. A stringent test of the model was performed by reconstructing the large-scale interplanetary magnetic field from the sun to beyond 5 AU and showing that the model simultaneously fits the observed Jovian electron event onsets and durations near Earth, at Pioneer 11 at 3.7 AU and at Pioneer 10 at 5.2 AU.

Figure 11 shows an idealization of the very regular large-scale structure of the interplanetary medium that was observed during the decline to minimum of Solar Cycle 20. The light areas in the figure represent the relatively undisturbed plasma of high speed solar wind streams which are approximated as scatter-free regions in the model while the shaded areas represent the solar wind stream interaction regions which form diffusive media in the models. This picture of Jovian electron propagation predicts well defined relationships between the observed electron profile and solar wind structure that depend on the observers position within the heliosphere. These relationships, which have been confirmed by the observations at earth and on Pioneers 10 and 11 out to ~ 10 AU are summarized in Figure 12. The three rows represent observer positions: (a) near earth on the bottom row, (b) between earth and Jupiter in the middle row and, (c) beyond Jupiter in the top row. The lines labelled V and E represent the predicted relationships between solar wind velocity and Jovian electron time histories, respectively. The shading signifies the region in which the electron intensities are expected to be above the detector threshold.

3. CONCLUSIONS AND FUTURE EFFORT

The scientific results obtained over the past two years offer us new insights into improving prediction techniques for energetic particle event histories and geomagnetic disturbances. In particular, we have new ideas, drawn from observation and quantified by theory, on emission of plasma and energetic particles from the corona into the interplanetary medium. We have simple but accurate approximations for plasma and energetic particle transport in the inner heliosphere, and we have proposed a new model for the propagation of particles in the outer heliosphere.

During the final year of this contract, we will make use of the opportunity offered us by the invitation to participate fully in the *International Solar-Terrestrial Predictions Workshop* (to be held in Boulder, April 1979), to convert our ideas into improved prediction algorithms which may then be evaluated by ourselves and our colleagues.

REFERENCES

Gold, R. E. and E. C. Roelof, Jovian electron propagation via solar wind stream interaction regions, *J. Geophys. Res., 84,* submitted 1978.

Hanson, J. M. and E. C. Roelof, Synoptic charts of large-scale coronal x-ray structure during Skylab, April 1973-February 1974, *Preprint JHU/APL 78-05,* submitted to UAG Special Reports, WDC-A, 1978.

Hanson, J. M., R. E. Gold and E. C. Roelof, Solar activity charts for Carrington Rotations 1600-1611, *Preprint JHU/APL 78-06,* submitted to UAG Special Reports, WDC-A, 1978.

Levine, R. H. and E. C. Roelof, Recurrent minima in solar energetic particle fluxes and their association with coronal magnetic structure, *EOS, 58,* 1204, 1977.

Mitchell, D. G., E. C. Roelof and J. H. Wolfe, Latitude dependence of solar wind velocity observed $\geq$ 1 AU, *J. Geophys. Res., 84,* submitted 1978.

McIntosh, P. S., Annotated atlas of H_α Synoptic Charts for Solar Cycle 20, 1964-1974, *World Data Center A, UAG Special Report,* (NOAA, eds), 1978.

Roelof, E. C. and R. E. Gold, Prediction of solar energetic particle event histories using real-times particle and solar wind measurements, Proc. *NATO/AGARD Symposium "Operational Modeling of the Aerospace Propagation Environment"* (Ottawa), in press, 1978.

Roelof, E. C., S. M. Krimigis and R. E. Gold, Coronal propagation and storage of energies $\sim$ 1 MeV/nucleon, in *A Close-up of the Sun,* ed. M. Neugebauer and R. W. Davies, Jet Propulsion Laboratory (Pasadena) Publication 78-10, 197, 1978.

Roelof, E. C., S. M. Krimigis, J. T. Nolte and J. M. Davis, Energetic solar particle events in 1965: Relationship to coronal magnetic structure, *J. Geophys. Res., 84,* submitted 1978.

Zwickl, R. D. and E. C. Roelof, Interplanetary propagation of < 1 MeV protons in non-impulsive energetic particle events, *J. Geophys. Res., 84,* submitted 1978.

Zwickl, R. D., E. C. Roelof and R. E. Gold, Z-rich solar particle event characteristics 1972-1976, *Astrophys. J., 225,* 281, 1978.

FIGURE CAPTIONS

FIGURE 1 Schematic representation of the heliosphere and the regime investigated in each of the studies conducted under this contract during the past years.

FIGURE 2 Solar Activity Chart for Carrington Rotation 1604. The H_α importance and brightness of solar flares is represented by the size and color of the dots on the visible region of the sun. Associated x-ray and radio burst intensities are represented by the spikes surrounding the flare circles as indicated in the legend. The energetic particle intensity stripe is plotted along the trajectory of the connection longitude of earth. McMath plage region numbers and their location in the northern or southern hemisphere are indicated along the bottom of the figure.

FIGURE 3a From annotated Atlas of H_α Synoptic Charts for Solar Cycle 20 (1964-1974). *McIntosh (1978).*

FIGURE 3b X-ray loop end points, x-ray plages (striped), and coronal holes (stippled). *Hanson and Roelof (1978)*

FIGURE 3c Superposition of Figures 3a and 3b.

FIGURE 4 Coronal structure in the vicinity of a small equatorial coronal hole *(Levine and Roelof, 1978).* Center: H_α inferred neutral lines and soft x-ray loops. Upper Left: open field lines originating on a 2.6 $R_\odot$ source surface calculated from a potential field. Upper Right: closed field lines from the same calculation.

FIGURE 5 Quasi-stationary energetic particle population above a coronal hole in August 1973. Lower: H_α absorbtion feature and coronal hole (from Figure 4) in heliographic coordinates. Upper: 1.9-4.5 MeV hourly-averaged proton fluxes "mapped back" to their estimated high coronal emission longitudes using simultaneous measurements of solar wind velocity on the IMP-7 spacecraft *(Levine and Roelof, 1978).*

FIGURE 6 Topographical map of the observed solar and interplanetary phenomena for the average Z-rich event shown as a function of radial distance and heliographic longitude. Included are the approximate locations of the solar flare active region, the coronal transition region denoted by the Alfvén critical surface, the fast and slow speed solar wind compression and rarefaction region (shaded) and the observed Z-rich event.

FIGURE 7 Panels consist of segments of H_α Synoptic Charts, with regions of well-defined negative magnetic polarity shaded. Most likely active region particle sources are marked by heavy dots. Regions of escape of energetic particles are marked by bars at the heliographic latitude of Mariner 4, with positive (vertical lines), negative (horizontal lines) or mixed (both) interplanetary polarity also indicated. Observed boundaries of escape regions are shown with vertical edges, while boundaries not observable because of temporal changes in particle intensities have pointed ends. Solar wind "dwells" (i.e., eastern boundaries of solar wind stream sources) are marked by heavy brackets (velocity > 400 km/s) or curved lines (velocity < 400 km/s) which are dashed for temporal streams.

FIGURE 8 Inferred velocity structure relative to the coronal hole boundaries on Rotation 1610. The structure to the right of the coronal hole cannot be accurately deduced due to stream-stream interactions. To the left (east) the Pioneer 11 velocities drop much more quickly than the IMP 7/8 velocities. The structure sketched is consistent with the observations (including the interplanetary magnetic field polarity agreement with that in the hole), but other geometries are not excluded.

FIGURE 9 Scatter plot of the calculated $\underline{E} \times \underline{B}$ drift anisotropy $\underline{\eta}_\perp$ versus the measured anisotropy component perpendicular to the magnetic field direction $\underline{\xi}_\perp$ in geocentric solar ecliptic coordinates. The $\underline{\xi}_\perp$ and $\underline{\eta}_\perp$ data show an amazingly strong correlation which suggests that the propgation of low energy protons is well described by collimated convection.

FIGURE 10 Examples of solar-wind/connection-longitude effects on a steady symmetric coronal particle injection: (a) velocity constant; velocity rise (b) early or (c) late in particle event. Lower panel (d) gives solar connection longitude at observation times t = 1, 2, 3, 4 and 5 days.

FIGURE 11 Idealization of the large-scale structure of the interplanetary medium during the period of very stable solar wind structure, 1972-1975. The white areas represent the solar wind streams while the shading represents the stream interaction regions which thicken with radial distance and eventually merge. The orbits of Earth and Pioneers 10 and 11 are shown in a fixed-Jupiter-Sun-line system in which the pinwheel completes one rotation in ~ 26 days. The Earth takes ~ 13 months to complete one orbit in this system and its positions during the early, middle and late Jovian electron seasons are indicated.

FIGURE 12 Schematic representation of the inter-relationships between solar wind velocity and Jovian electrons predicted by the model for near-Earth, Pioneers inside 5 AU and Pioneer 10 beyond ~ 6 AU. The curves labelled V and E represent the time histories of solar wind velocity and electrons respectively. The shading approximates the electron selection criteria for a Jovian event. with Figure 2.

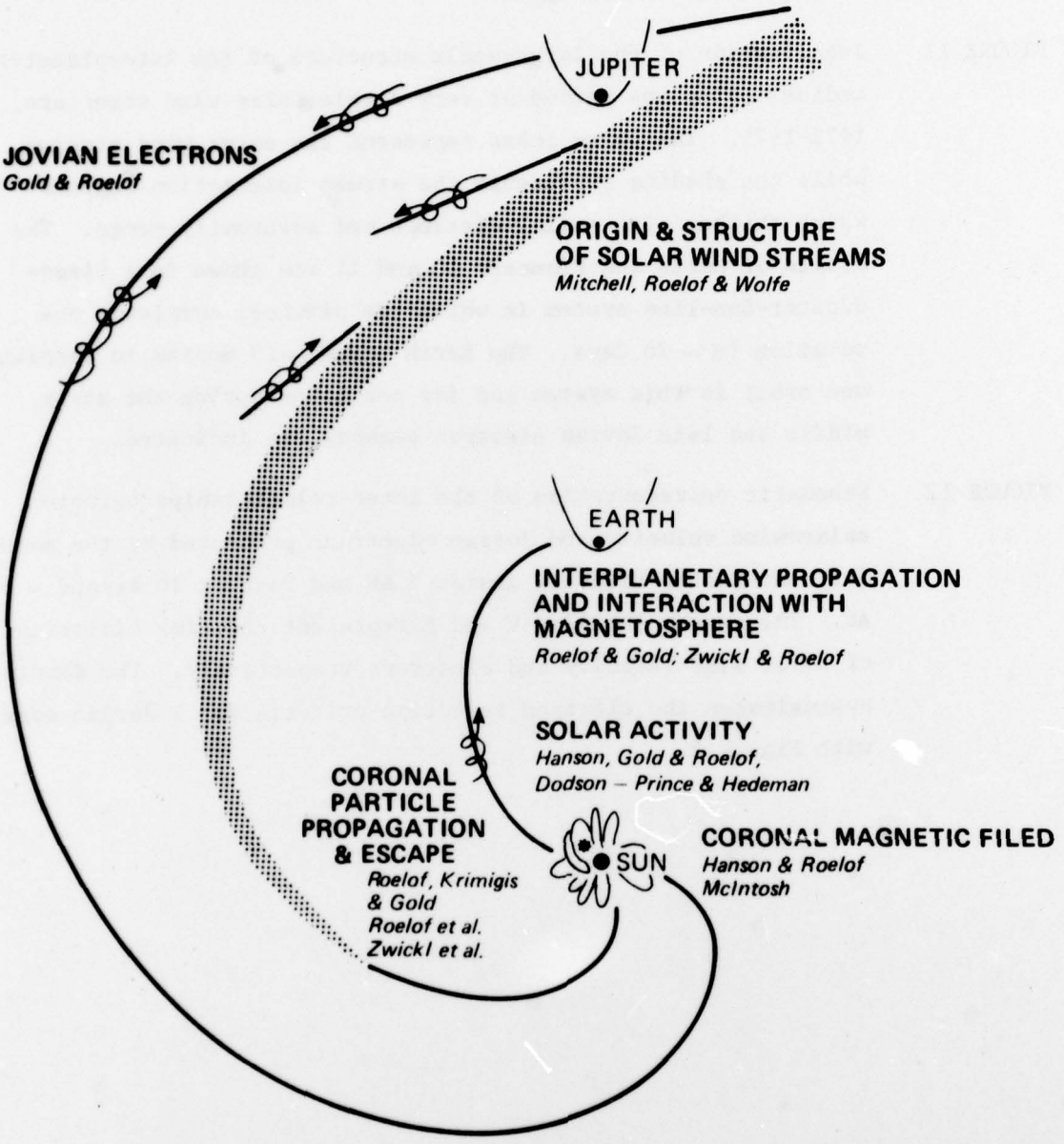
JUPITER
JOVIAN ELECTRONS
Gold & Roelof
ORIGIN & STRUCTURE
OF SOLAR WIND STREAMS
Mitchell, Roelof & Wolfe
EARTH
INTERPLANETARY PROPAGATION
AND INTERACTION WITH
MAGNETOSPHERE
Roelof & Gold; Zwickl & Roelof
SOLAR ACTIVITY
Hanson, Gold & Roelof,
Dodson – Prince & Hedeman
CORONAL
PARTICLE
PROPAGATION
& ESCAPE
Roelof, Krimigis
& Gold
Roelof et al.
Zwickl et al.
SUN
CORONAL MAGNETIC FILED
Hanson & Roelof
McIntosh

FIGURE 1

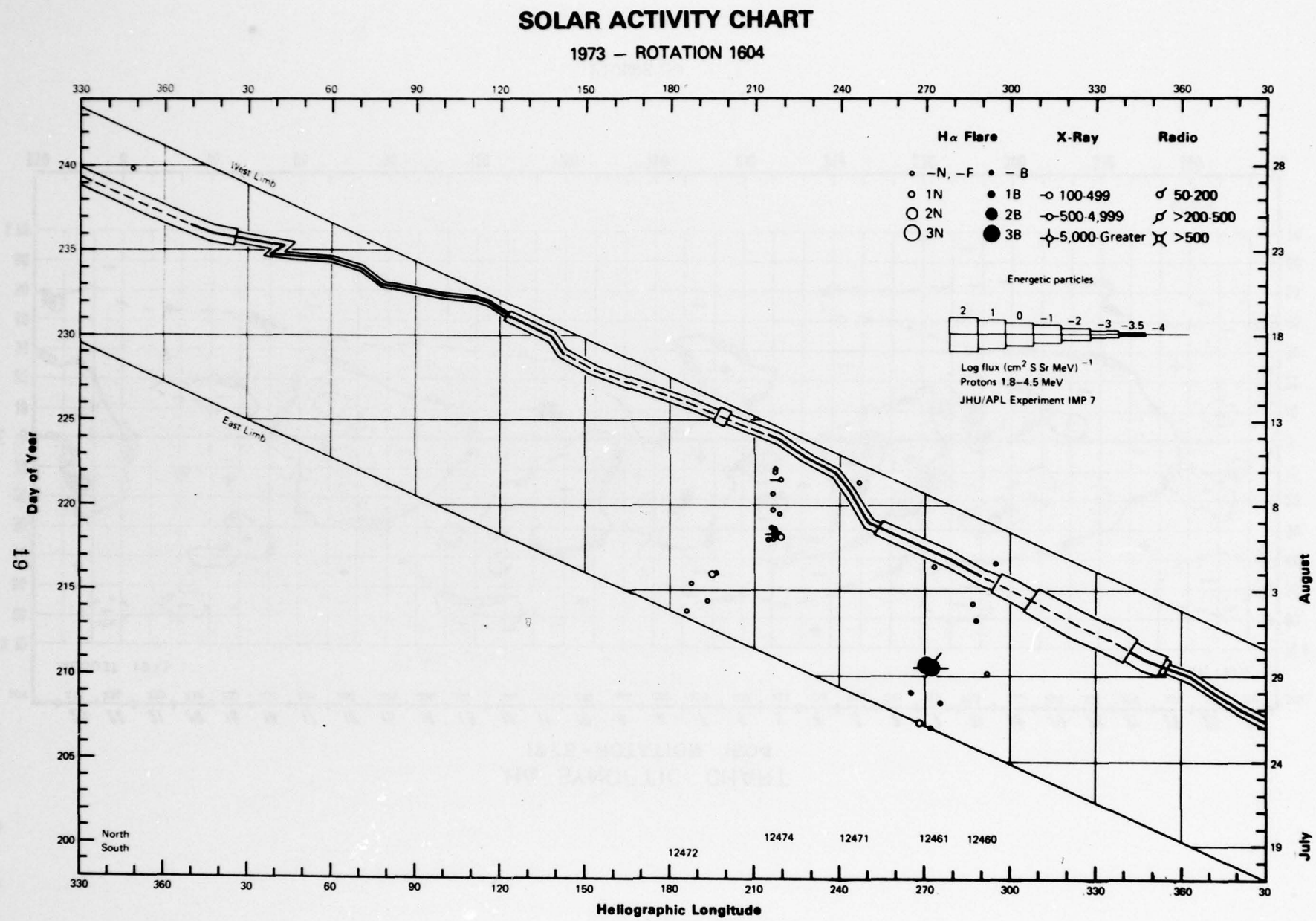
SOLAR ACTIVITY CHART
1973 — ROTATION 1604
Hα Flare
X-Ray
Radio
–N, –F
– B
1N
1B
100-499
50-200
2N
2B
500-4,999
>200-500
3N
3B
5,000-Greater
>500
Energetic particles
2 1 0 –1 –2 –3 –3.5 –4
Log flux (cm² S Sr MeV)⁻¹
Protons 1.8–4.5 MeV
JHU/APL Experiment IMP 7
West Limb
East Limb
North
South
12472
12474
12471
12461
12460
Day of Year
19
July
August
Heliographic Longitude
330 360 30 60 90 120 150 180 210 240 270 300 330 360 30
240 235 230 225 220 215 210 205 200
28 23 18 13 8 3 29 24 19

FIGURE 2

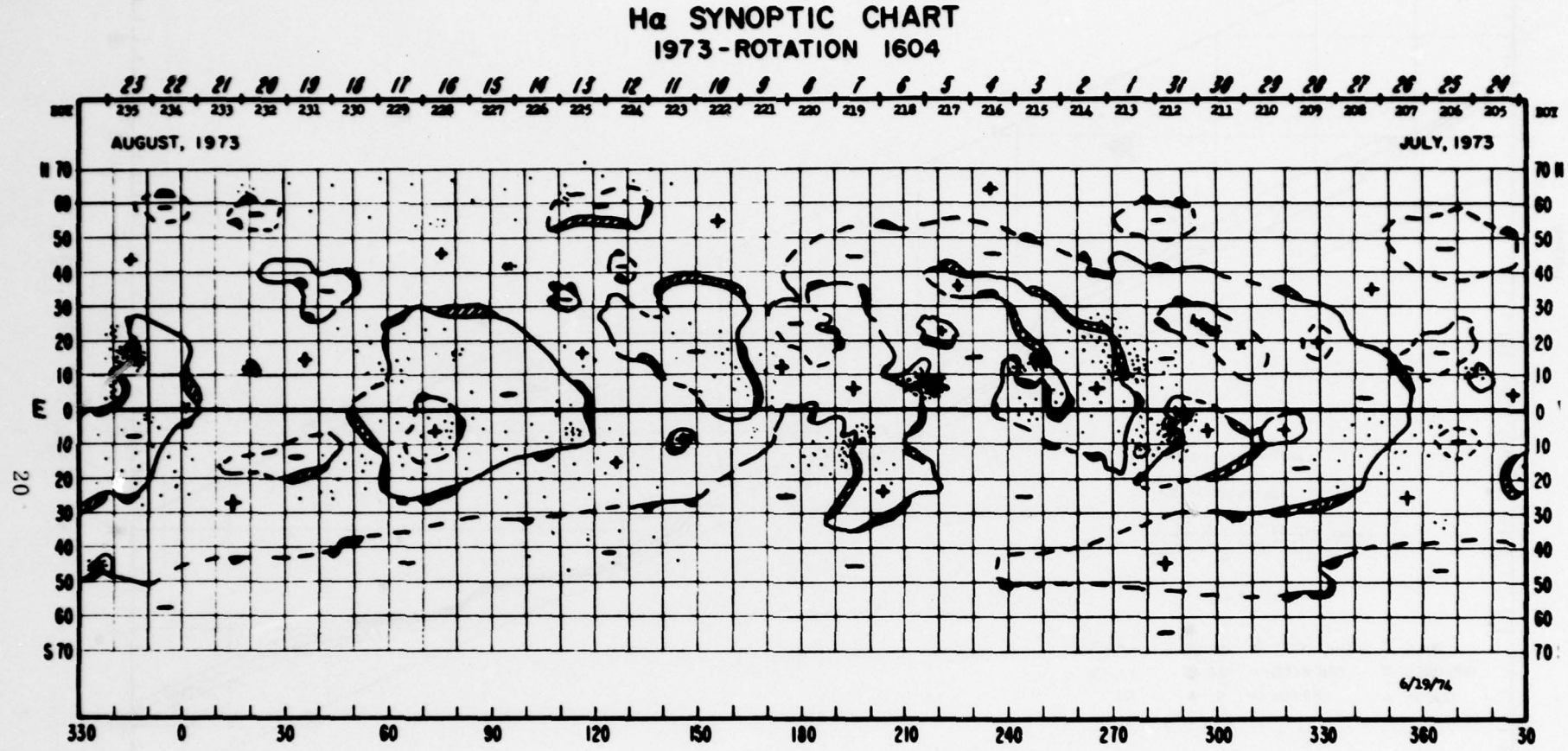
Hα SYNOPTIC CHART
1973 - ROTATION 1604
AUGUST, 1973
JULY, 1973
6/19/74

FIGURE 3a

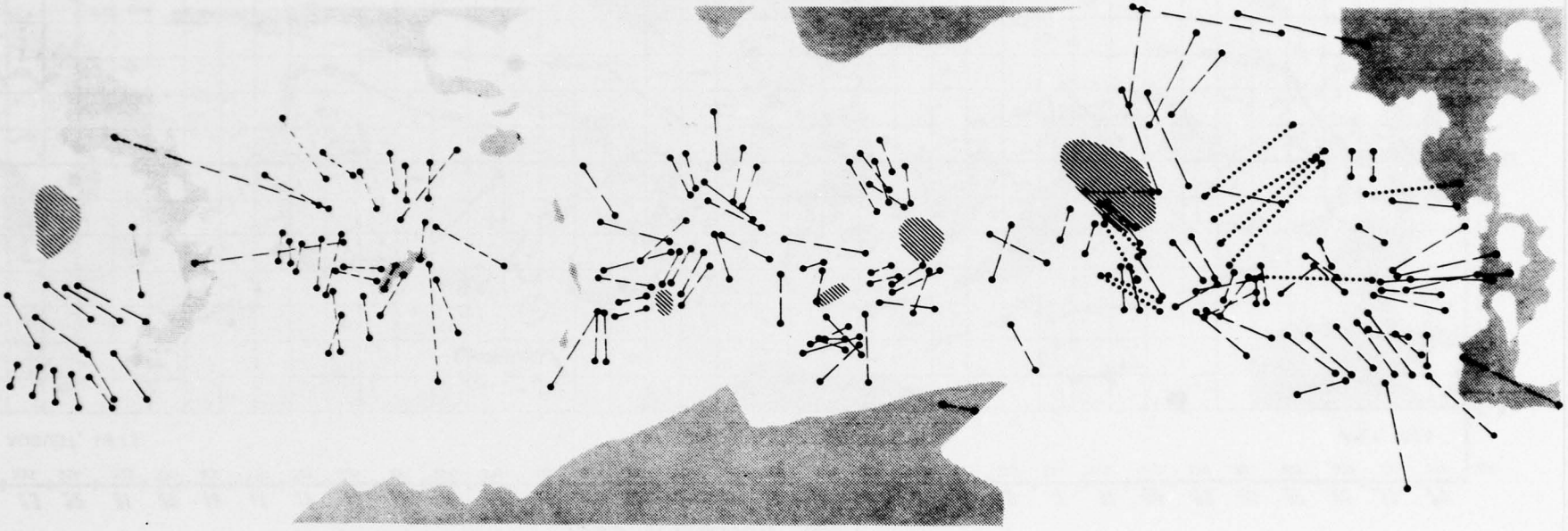

FIGURE 3b

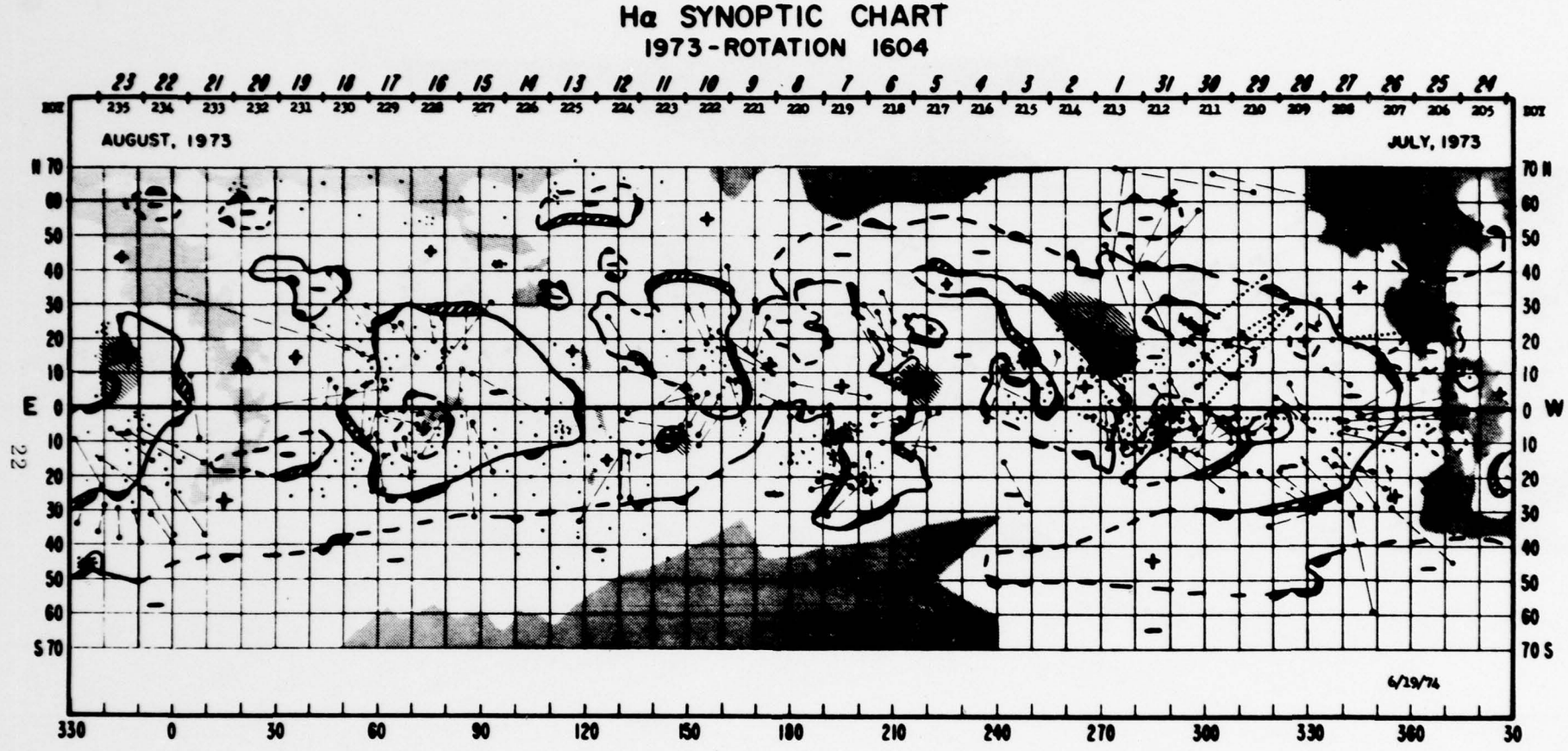
Hα SYNOPTIC CHART
1973 - ROTATION 1604
AUGUST, 1973
JULY, 1973
6/19/74

FIGURE 3c

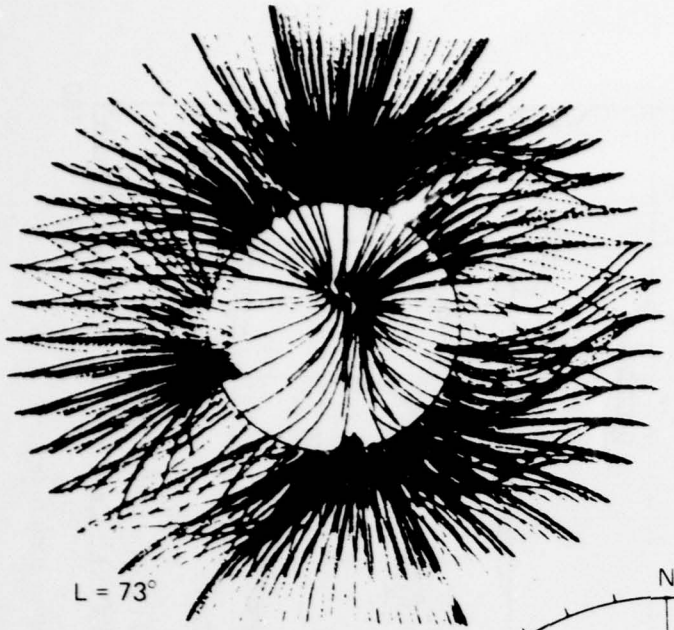

Open field lines originating on source surface (2.6 $R_\odot$) (HCO/SAO)

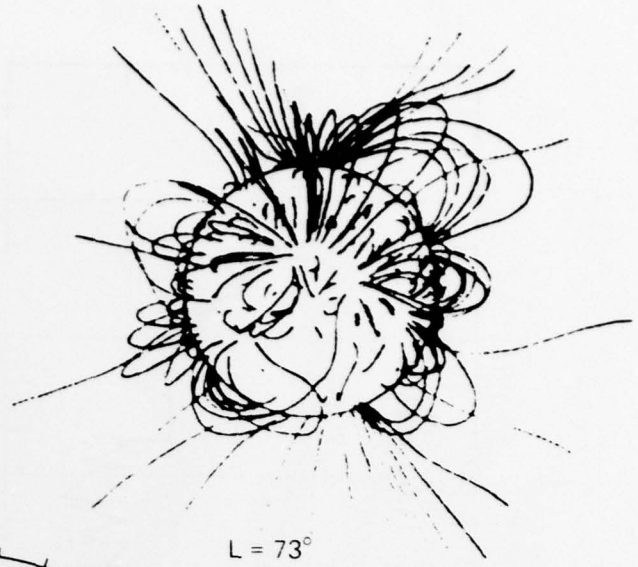

Weak field *structure* (18 zones, 36 sectors) (HCO/SAO)

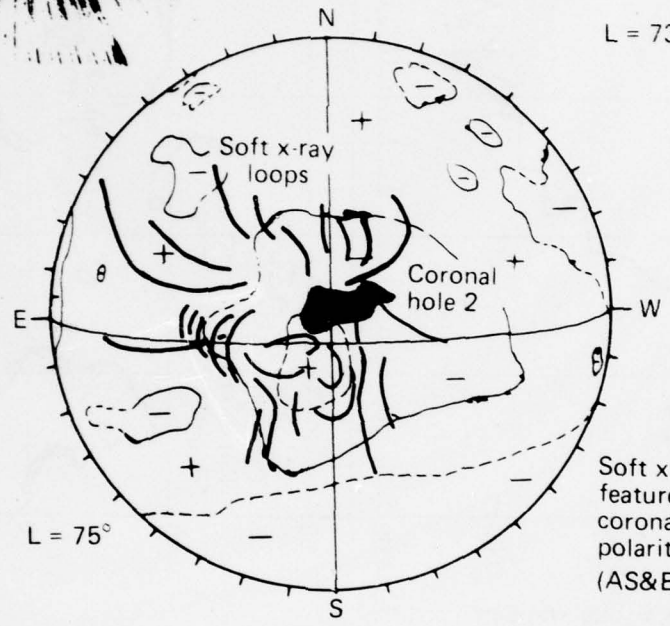

Soft x-ray features and coronal magnetic polarity regions (Hα) (AS&E/NOAA)

FIGURE 4

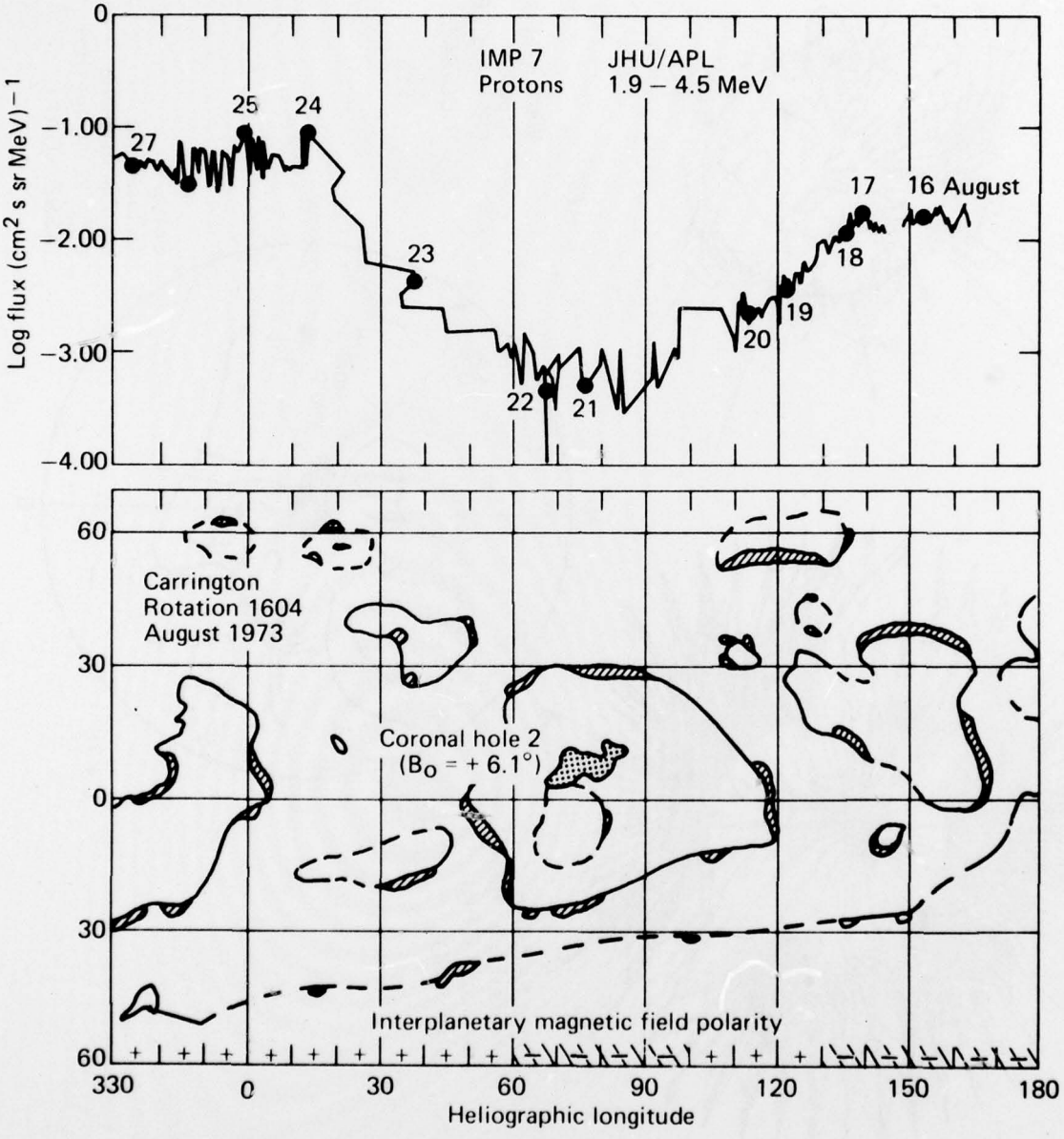
IMP 7
Protons
JHU/APL
1.9 – 4.5 MeV
Log flux (cm² s sr MeV)⁻¹
0
−1.00
−2.00
−3.00
−4.00
27
25
24
23
22
21
20
19
18
17
16 August
Carrington
Rotation 1604
August 1973
Coronal hole 2
(B₀ = + 6.1°)
60
30
0
30
60
Interplanetary magnetic field polarity
330
0
30
60
90
120
150
180
Heliographic longitude

FIGURE 5

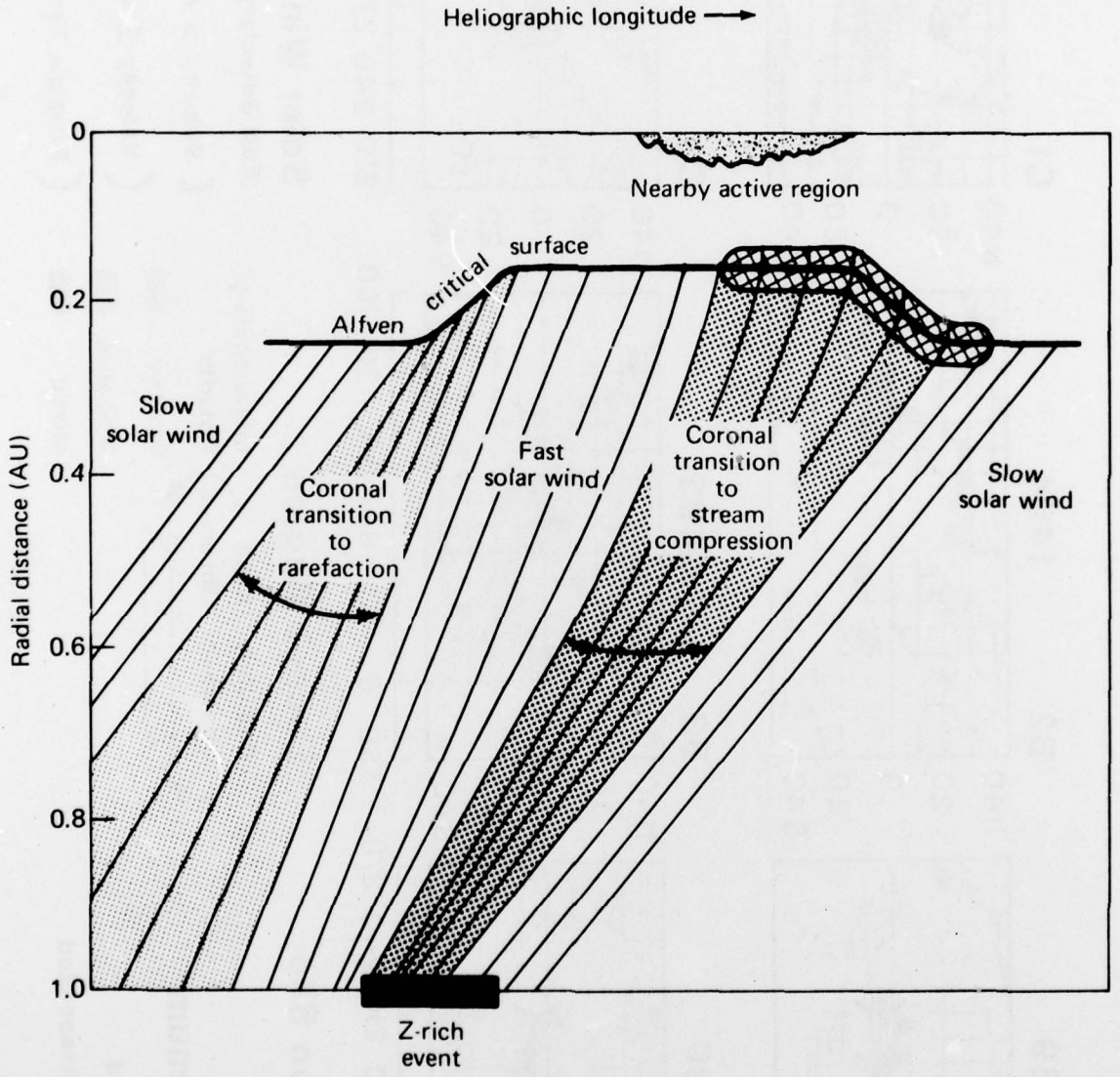
Heliographic longitude
0
0.2
0.4
0.6
0.8
1.0
Radial distance (AU)
Nearby active region
surface
critical
Alfven
Slow
solar wind
Coronal
transition
to
rarefaction
Fast
solar wind
Coronal
transition
to
stream
compression
Slow
solar wind
Z-rich
event

FIGURE 6

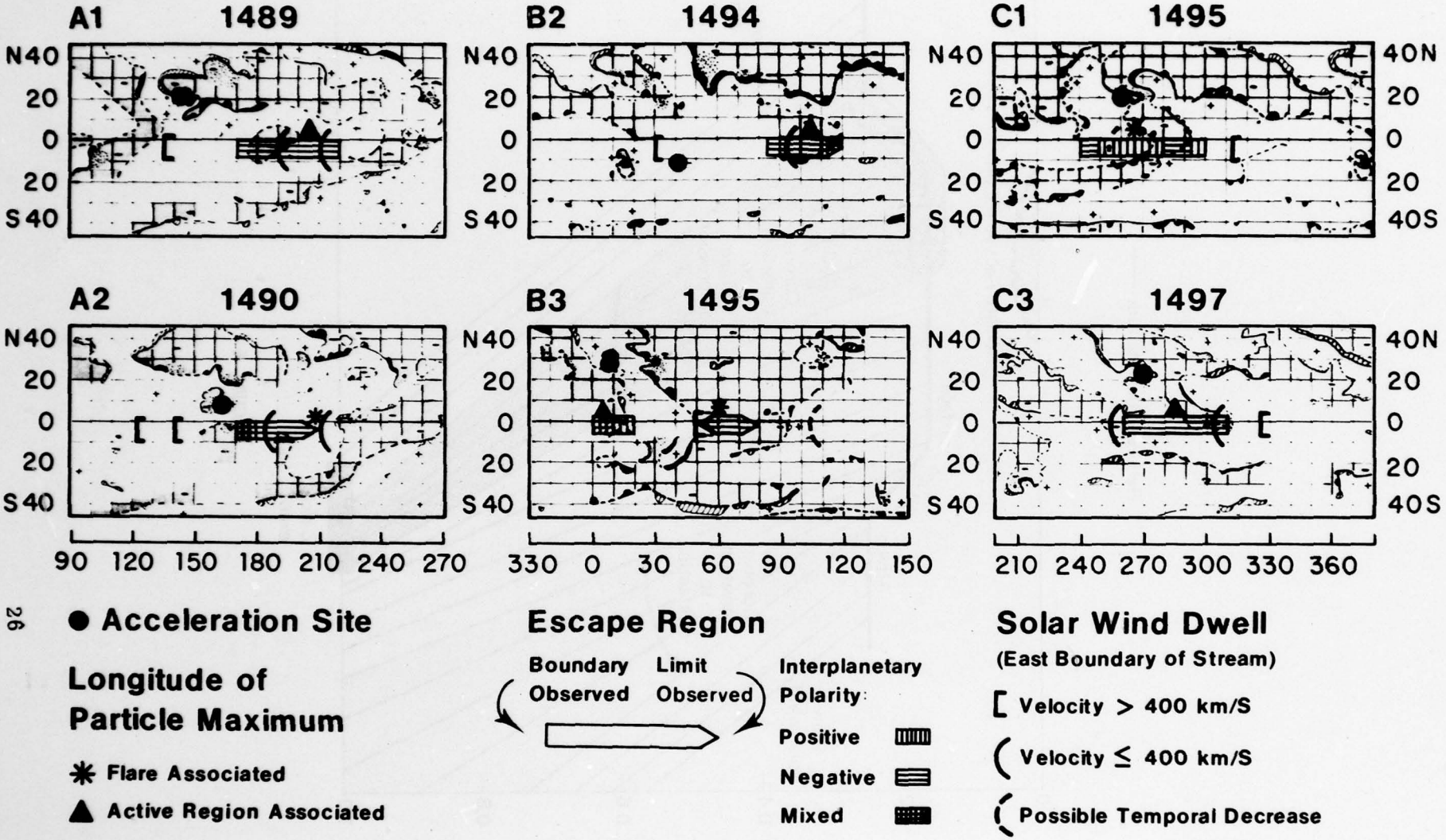
A1 1489
B2 1494
C1 1495
A2 1490
B3 1495
C3 1497
N40
20
0
20
S40
40N
40S
90 120 150 180 210 240 270
330 0 30 60 90 120 150
210 240 270 300 330 360
● Acceleration Site
Longitude of Particle Maximum
✱ Flare Associated
▲ Active Region Associated
Escape Region
Boundary Observed
Limit Observed
Interplanetary Polarity:
Positive
Negative
Mixed
Solar Wind Dwell
(East Boundary of Stream)
[Velocity > 400 km/S
(Velocity ≤ 400 km/S
(Possible Temporal Decrease

FIGURE 7

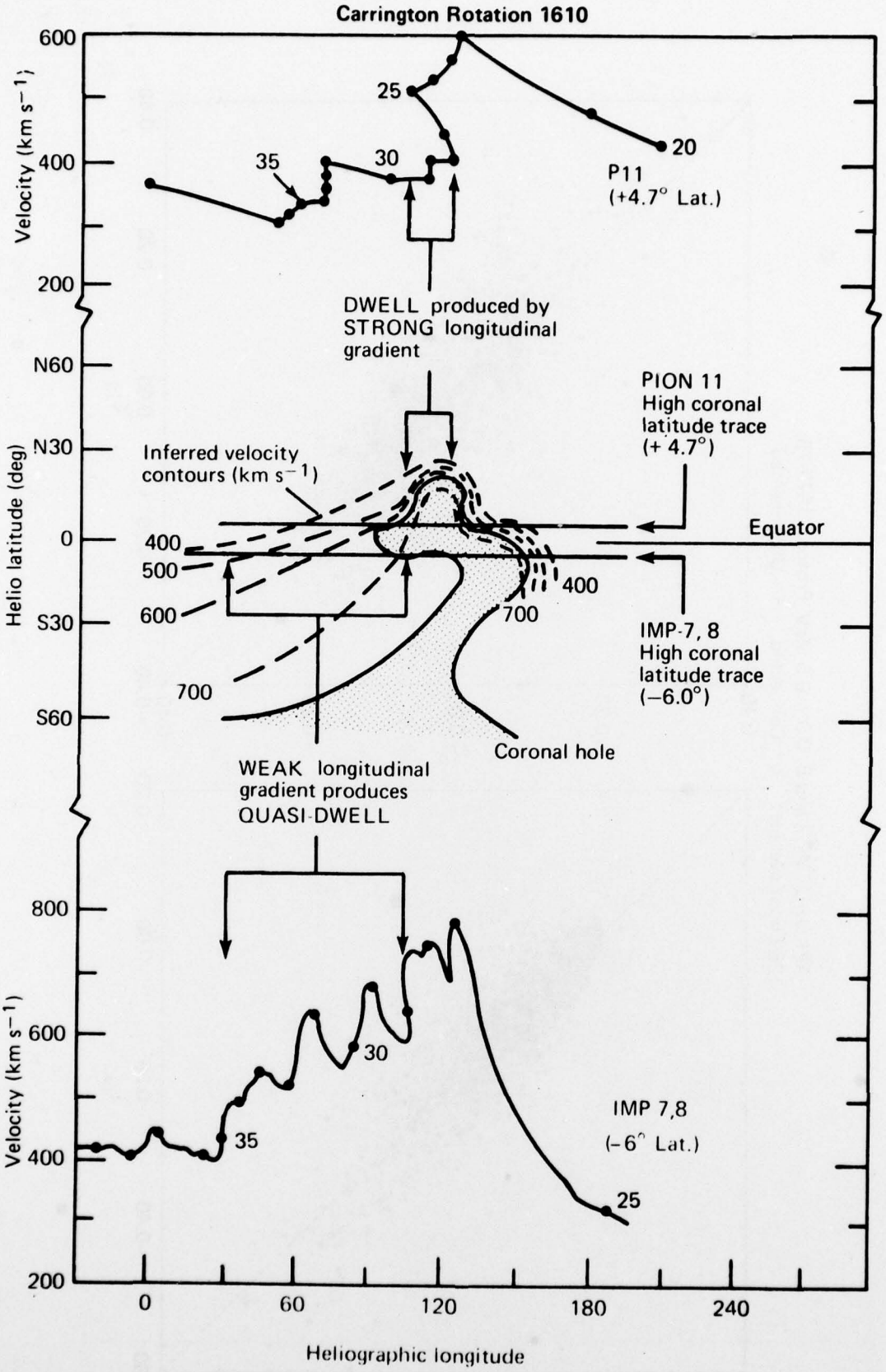
Carrington Rotation 1610
Velocity (km s⁻¹)
600
400
200
25
35
30
20
P11
(+4.7° Lat.)
DWELL produced by
STRONG longitudinal
gradient
N60
N30
0
S30
S60
Helio latitude (deg)
PION 11
High coronal
latitude trace
(+ 4.7°)
Inferred velocity
contours (km s⁻¹)
Equator
400
500
600
700
400
700
IMP-7, 8
High coronal
latitude trace
(−6.0°)
Coronal hole
WEAK longitudinal
gradient produces
QUASI-DWELL
800
600
400
200
Velocity (km s⁻¹)
30
35
IMP 7,8
(−6° Lat.)
25
0
60
120
180
240
Heliographic longitude

FIGURE 8

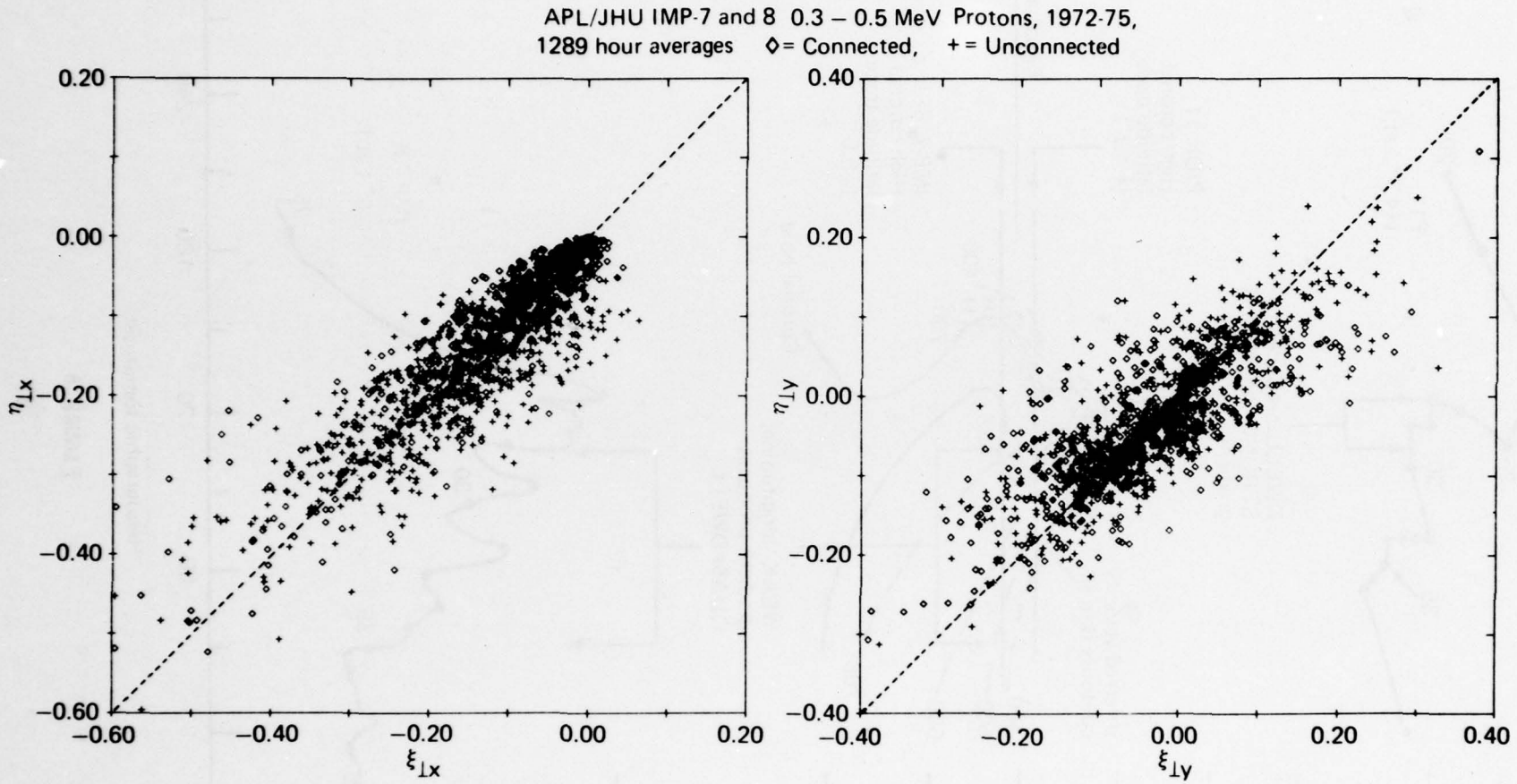
APL/JHU IMP-7 and 8 0.3 – 0.5 MeV Protons, 1972-75,
1289 hour averages ◇= Connected, + = Unconnected
0.20
0.00
−0.20
−0.40
−0.60
$\eta_{\perp x}$
−0.60
−0.40
−0.20
0.00
0.20
$\xi_{\perp x}$
0.40
0.20
0.00
−0.20
−0.40
$\eta_{\perp y}$
−0.40
−0.20
0.00
0.20
0.40
$\xi_{\perp y}$

FIGURE 9

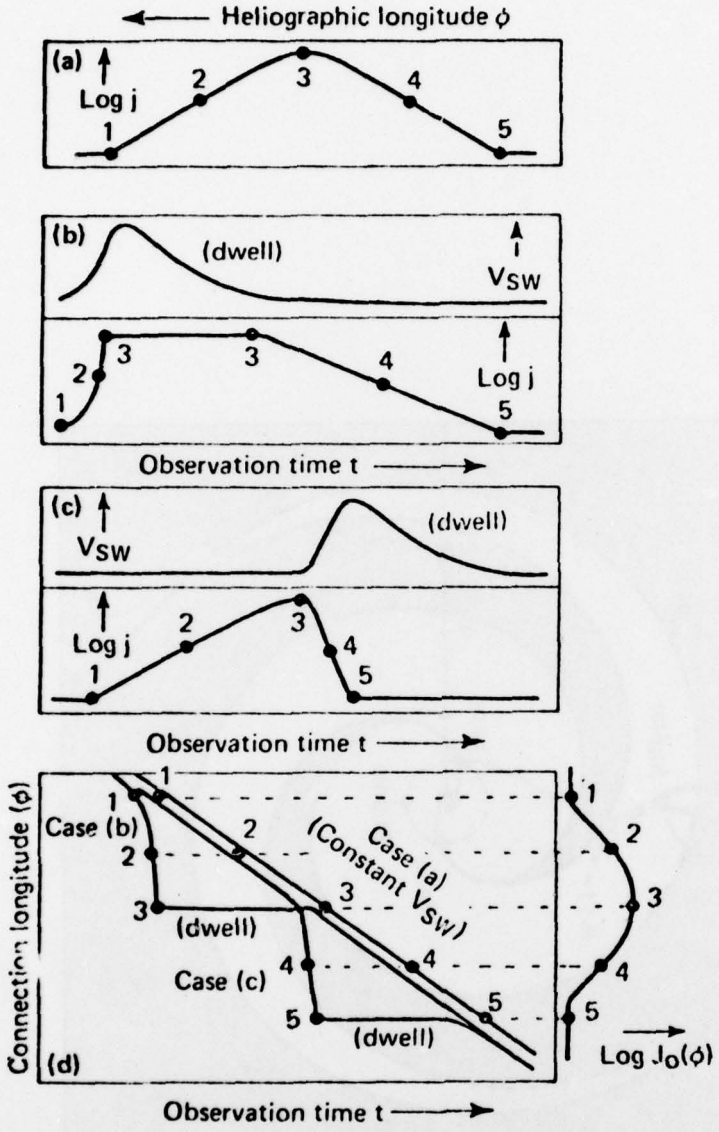
Heliographic longitude ϕ
(a)
Log j
1
2
3
4
5
(b)
(dwell)
V_{SW}
Log j
Observation time t
(c)
V_{SW}
(dwell)
Log j
Observation time t
Connection longitude (ϕ)
Case (b)
(dwell)
Case (c)
(dwell)
Case (a)
(Constant V_{SW})
(d)
Log $J_o(\phi)$
Observation time t

FIGURE 10

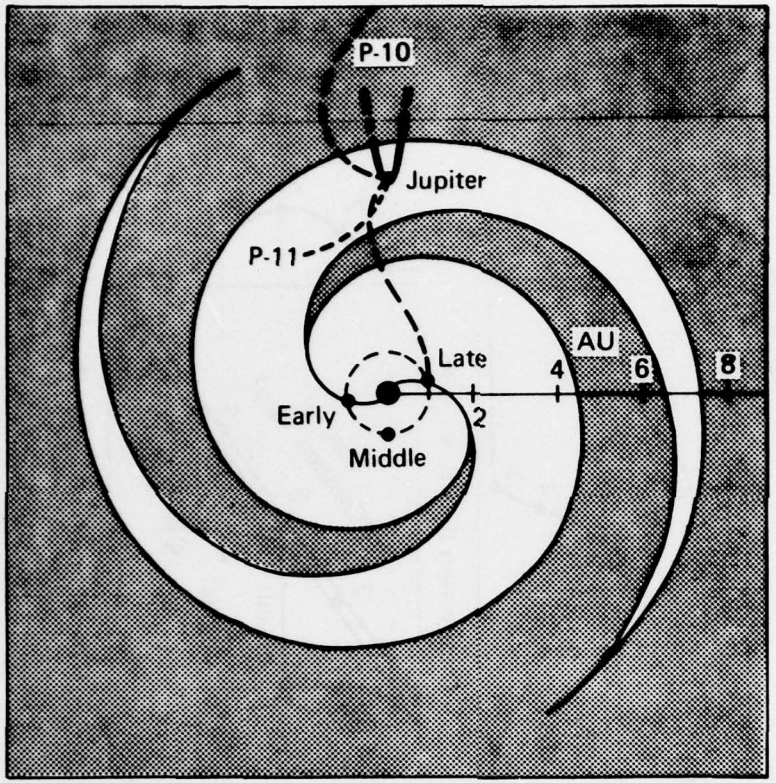

FIGURE 11

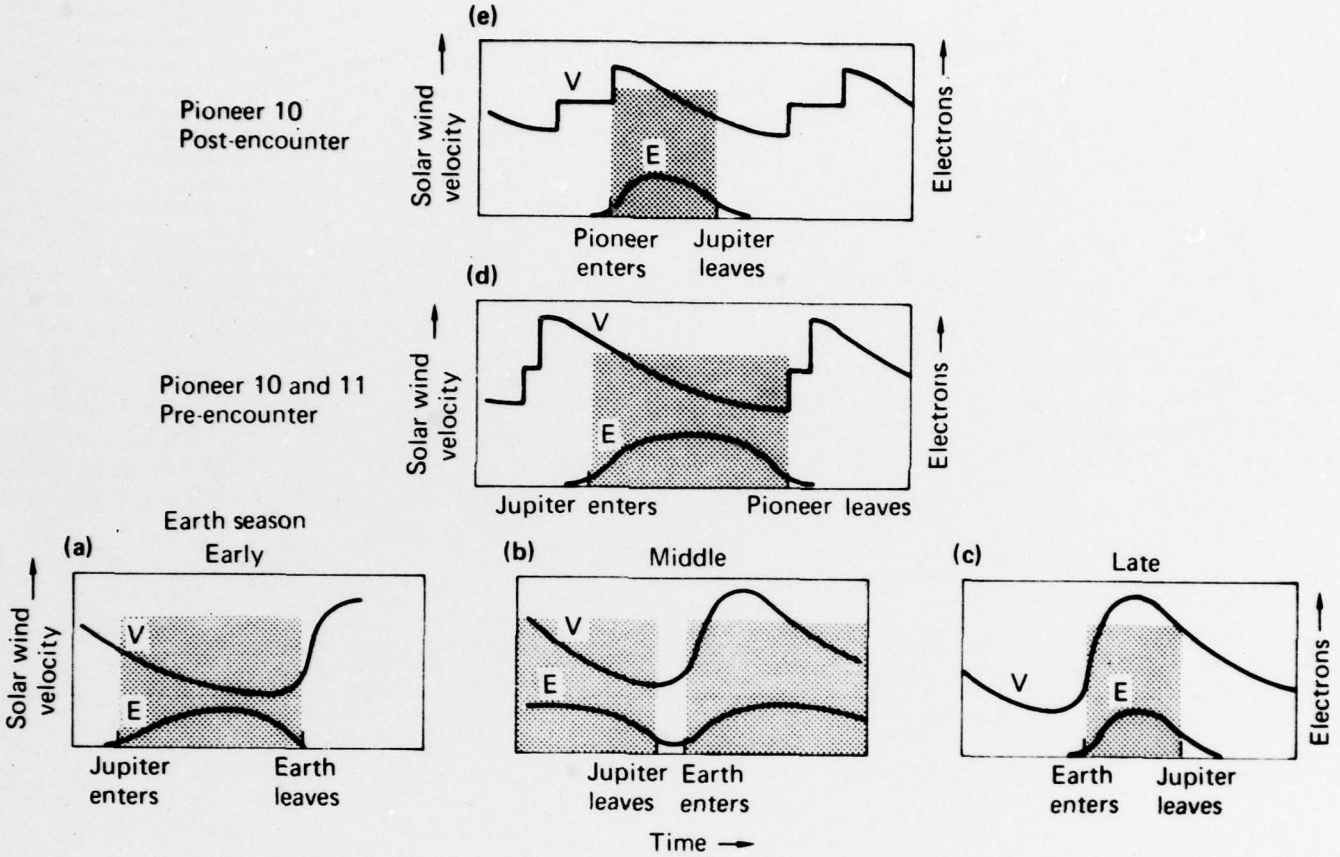
(e)
Pioneer 10
Post-encounter
Solar wind velocity
Electrons
V
E
Pioneer enters
Jupiter leaves
(d)
Pioneer 10 and 11
Pre-encounter
Solar wind velocity
Electrons
V
E
Jupiter enters
Pioneer leaves
Earth season
(a)
Early
Solar wind velocity
V
E
Jupiter enters
Earth leaves
(b)
Middle
V
E
Jupiter leaves
Earth enters
(c)
Late
V
E
Electrons
Earth enters
Jupiter leaves
Time

FIGURE 12